

Recent experimental and analytic progress in the Japan Atomic Energy Research Institute Tokamak-60 Upgrade with W-shaped divertor configuration*

H. Shirai^{†,a)} and the JT-60 Team^{b)}

Japan Atomic Energy Research Institute, Naka-machi, Naka-gun, Ibaraki-ken, 311-0193, Japan

(Received 17 November 1997; accepted 9 February 1998)

The Japan Atomic Energy Research Institute (JAERI) completed the divertor modification of the JAERI Tokamak-60 Upgrade (JT-60U) [Y. Koide and the JT-60 Team, *Phys. Plasmas* **4**, 1623 (1997)] in June, 1997, and experiments with the W-shaped pumped divertor have been carried out. The helium exhaust was demonstrated in the steady state by using helium neutral beam injection (NBI). The ratio of the effective particle confinement time of helium to the energy confinement time, τ_{He}^*/τ_E , became about 4 and the obtained enrichment factor of helium in the divertor was about 1. The high confinement mode (H-mode) plasma with edge localized mode (ELM) was sustained for 9 s with a confinement–enhancement factor (H factor) of ~ 1.7 . No increase of recycling and carbon impurity density was observed with the integrated NBI input energy of 203 MJ. In the reversed shear (RS) experiments, a quasi-steady-state ELMy H mode was achieved with an H factor ~ 2.4 . The stability of high- n toroidal drift modes was analyzed in the RS plasma. The $E \times B$ shearing rate became of the same order of magnitude as the linear growth of the dominant mode around the internal transport barrier. The semiglobal structure of radial transport was analyzed by the toroidal geometry particle simulation code. The discontinuity in the electrostatic potential occurred at the q_{min} region and radial transport was reduced. © 1998 American Institute of Physics. [S1070-664X(98)95405-2]

I. INTRODUCTION

The Japan Atomic Energy Research Institute Tokamak-60 Upgrade (JT-60U)¹ has been achieved high-performance plasmas in various operational modes such as hot ion high confinement mode (H-mode),² high- β_p H-mode,³ reversed shear (RS) mode⁴ and so forth, and contributed to International Thermonuclear Experimental Reactor (ITER)⁵ physics R&D from various physical points of view. In 1996, the fusion triple product, $n_D(0)\tau_E T_i(0) = 1.5 \times 10^{21} \text{m}^{-3} \text{s keV}$, and the deuterium–deuterium (D–D) neutron emission rate of $5.2 \times 10^{16} \text{s}^{-1}$ was obtained in high- β_p H mode⁶ and the equivalent deuterium–tritium (D–T) fusion amplification factor, $Q_{DT}^{eq} = 1.05$ was realized in the reversed shear operation.⁷

Because the performance achieved above was obtained in the transient phase, the long sustainment or the quasi-steady-state operation of high-performance plasmas becomes important in JT-60U experiments. In order to accomplish this aim, approaches of research from both divertor plasma physics and main plasma physics are necessary.

For the long duration operation, careful conditioning of the divertor plasmas becomes more and more essential. During the long neutral beam injection (NBI) heating phase, for example, the degradation of the main plasma confinement

and the influx of carbon impurity occurred because of the high heat flux toward the divertor plates.⁸ Formation of the partial detached remote radiative divertor is necessary for the heat control. The prompt exhaust of helium ash and the reduction of impurity from the main plasma is also important for the steady-state operation. Suppression of the neutral backflow toward the main plasma in order to achieve better H-mode performance is also an essential subject. For these reasons the W-shaped pumped divertor system was installed in JT-60U in 1997 and experiments started from June, 1997. In this paper we deal with the recent experimental and analytic results since June, 1997.

The study of noninductive current drive by the negative ion based NBI (N-NBI: beam energy, E_b , up to 500 keV),⁹ the lower hybrid wave¹⁰ and the bootstrap current¹¹ have been carried out in JT-60U. Especially, N-NBI has a larger current drive efficiency compared with the positive ion based NBI (P-NBI: $E_b \sim 90$ keV).¹ In 1996 experiments, we obtained full noninductive current drive in a high- β_p H-mode plasma for 2.6 s with $\beta_N \sim 2.5$ and a confinement–enhancement factor (H factor) ~ 2.5 .¹² However, the higher H factor, β_N , $n_D(0)\tau_E T_i(0)$, and Q_{DT}^{eq} value were obtained only in the “transient” phase, and such plasmas ended by the major disruption.

Achievement of high performance for a long duration operation by the optimization of both the divertor and the main plasma by making the best use of the W-shaped pumped divertor is the central subject of the experiments in this year.

In Sec. II, the modified divertor is introduced. The re-

*Paper sFraII-2 Bull. Am. Phys. Soc. **42**, 2063 (1997).

[†]Invited speaker.

^{a)}Electronic mail: shiraih@fusion.naka.jaeri.go.jp

^{b)}See Appendix.

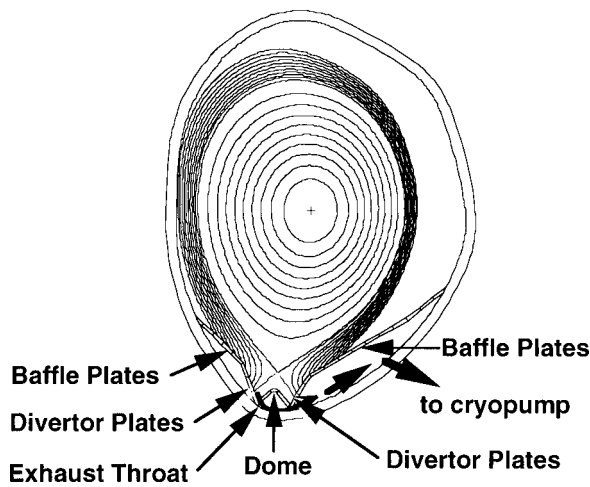


FIG. 1. Overview of the JT-60U W-shaped pumped divertor system.

sults of experiments related to the divertor pump such as helium exhaust and the long sustainment of the ELM (edge-localized mode) H mode are discussed there. In Sec. III, the experimental results of reversed shear plasmas are presented. The analysis of the microinstability around the internal transport barrier (ITB) by a toroidal kinetic microinstability analysis code and the reduced radial transport at the ITB region by a toroidal particle code are also shown. In Sec. IV, important subjects in ITER physics R&D, the halo current, and the Toroidal Alfvén Eigenmode (TAE), are shown. A summary of JT-60 experimental and analytic progress in this year and the future plan are shown in Sec. V.

II. W-SHAPED DIVERTOR EXPERIMENTS

A. Divertor modification

The poloidal cross section of JT-60U after the divertor modification is shown in Fig. 1. The new divertor has a W-shaped structure with the inner and the outer baffle plates, the 60° inclined divertor plates, and the center dome. In order to resist the high heat flux from the main plasma, carbon fiber composite (CFC) tiles are adopted for the divertor plates. This divertor configuration was designed and optimized by numerical simulations.¹³ Main features predicted by numerical simulations are as follows. The inclined divertor plates reduce the heat load and create high recycling, high-density, and low-temperature radiative divertor plasmas. The baffle plates reduce the backflow of neutral particles toward the main plasma. The dome reduces the carbon impurity flux toward the X point.

Figure 2 shows the enlarged poloidal cross section around the X point and the divertor region. There is an exhaust throat between the inner divertor plate and the dome. Particles in the divertor region are pumped from the private region, which is the same structure as the ITER design.¹⁴ The distance between the inner separatrix hit point and the dome is called “gap-in.” The gap-in can be changed by the plasma configuration (2–14 cm). The smaller gap-in is accompanied by the higher pump efficiency.

The comparison of the operational region before and after the divertor modification is summarized in Table I. The

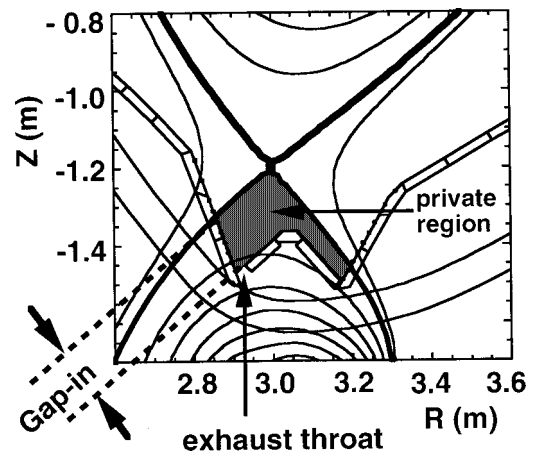


FIG. 2. The enlarged poloidal cross section around the X point and the divertor region.

dome was installed at the bottom of the vacuum vessel and the height of the X point became relatively higher than that of the open divertor. Since the maximum divertor coil current is the same, maximum plasma current is limited at 3 MA in order to keep the divertor configuration. Three P-NBI units were removed, but the attached cryopumps provide the pumping for the divertor. The power from N-NBI is planned to compensate for the decrease in the total P-NBI power.

From the view point of the above items, the operational region became slightly narrower. However, the modification of the JT-60U device made it more suitable to study the physics of divertor plasmas and optimize the operation by the heat control, particle control, and the impurity control in order to satisfy the performance of the ITER divertor.

The divertor particle pumping speed is adjustable by the opening in front of the cryopumps. The argon-frosted cryopump enables the demonstration of helium exhaust. Six gas puffing ports in total, four from the top of main plasma and two from behind the baffle plates, were installed.

B. Active fuel exhaust

The particle flux pumped out by the divertor pump was estimated by comparing a set of plasmas with and without the divertor pump. The balance of the particle flux can be expressed as $\Gamma_{NB}^W + \Gamma_{W/O}^{GP} = \Gamma_{WALL}^W + \Gamma_{PUMP}$ for with (W) divertor pump, and $\Gamma_{NB}^{W/O} + \Gamma_{W/O}^{GP} = \Gamma_{WALL}^{W/O}$ for without (W/O) divertor pump. Here Γ_{NB} and Γ_{GP} are influx to the plasma by NBI and the gas puff, respectively. Here Γ_{WALL} and Γ_{PUMP}

TABLE I. A comparison of the operational region for a W-shaped divertor and an open divertor.

	W-shaped divertor (1997)	Open divertor (1996)
Plasma current	2.5 MA 3.0 MA (design)	5 MA 6 MA (design)
P-NBI	11 units (~28 MW)	14 units (~37 MW)
Plasma volume	~85 m ³	~100 m ³
Gas puff port	6 (4: main, 2: divertor)	2
Divertor pump	Yes (three ports)	No
Helium pump	Argon frosted possible	Solid target boronization ¹⁵

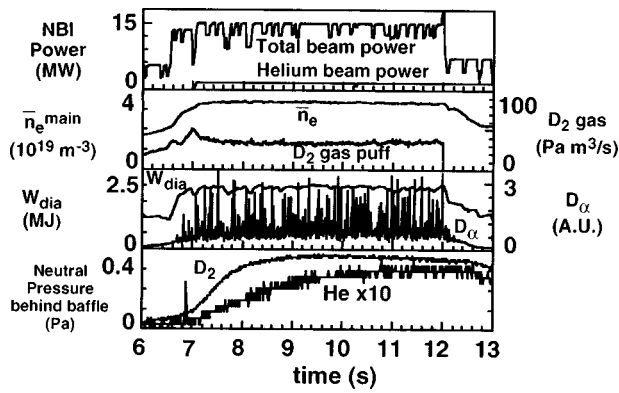


FIG. 3. Time evolution of the total NBI heating power, the helium beam power, the line-averaged electron density, the amount of deuterium gas puff, the diamagnetic stored energy, the intensity of divertor D_α , and the neutral pressure of deuterium and helium behind the outer baffle plate in the helium exhaust experiments.

are outflux pumped out by the wall and the divertor pump, respectively. The plasma density is kept at the same value in both discharges by the feedback control of gas puff fueling. The same NBI fueling is carried out, that is $\Gamma_{\text{NB}}^{\text{W}} = \Gamma_{\text{NB}}^{\text{W/O}}$. On the assumption of the same wall pumping in both discharges, that is $\Gamma_{\text{WALL}}^{\text{W}} = \Gamma_{\text{WALL}}^{\text{W/O}}$, the difference in the particle influx by the gas puff, $\Gamma_{\text{GP}}^{\text{W}} - \Gamma_{\text{GP}}^{\text{W/O}}$, in order to maintain the same plasma density, corresponds to the outflux by the divertor pump, Γ_{PUMP} . The ELMy H-mode plasma of $I_p = 1.5$ MA, $B_t = 3.5$ T, $\bar{n}_e = 4.3 \times 10^{19} \text{ m}^{-3}$, $P_{\text{NBI}} = 12$ MW, and the gap-in = 3.5 cm was examined. In the case with divertor pump, $\Gamma_{\text{NB}} = 4 \text{ Pa m}^3/\text{s}$, $\Gamma_{\text{GP}} = 20 \text{ Pa m}^3/\text{s}$, and $\Gamma_{\text{PUMP}} = 12.3 \text{ Pa m}^3/\text{s}$ was estimated. Thus, about half the fueled particles are removed by the divertor pump. This active fuel exhaust works quite well for the helium exhaust, the long sustainment of the ELMy H mode, and so forth, which are shown below.

C. Helium exhaust

The removal of helium ash from the main plasma is one of the essential subjects for the steady-state operation of fusion reactors. In the open divertor, helium removal from high- β_p ELMy H-mode plasmas was demonstrated by using the method of wall pumping by solid target boronization.¹⁵ The ratio of the effective particle confinement time of helium, τ_{He}^* , to the energy confinement time, τ_E , was 6–8.

The demonstration of helium removal by the divertor pump was carried out. The argon-frosted cryopump is used for this experiment. The ELMy H-mode plasma with $I_p = 1.4$ MA and $B_t = 3.5$ T is examined. The time evolution of this shot is shown in Fig. 3. Helium is injected into plasma by using two units of NBI. The beam power and beam energy of helium are 60 keV and 1.4 MW, respectively. The H factor and β_N are 1.3 and 1.0, respectively. The helium source is $1.5 \times 10^{20} \text{ s}^{-1}$, which is equivalent to the helium ash production by 80 MW α heating. The line-averaged electron density is kept constant during NBI heating by the feedback control of the deuterium gas puff. The stored energy and neutron emission rate is almost constant during NBI. The neutral pressure of both deuterium and helium behind the outer baffle plate saturates about 2 s after the beginning

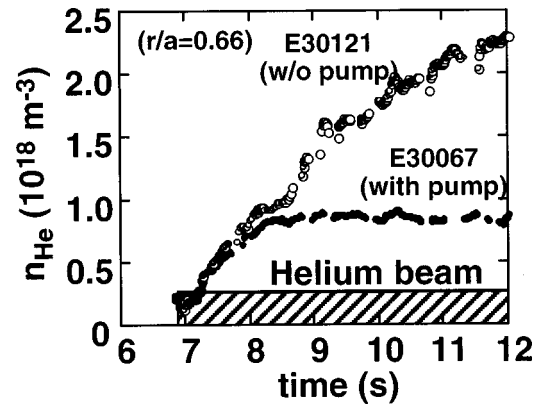


FIG. 4. Time evolution of helium density at $r/a=0.66$ with and without a divertor pump.

of helium beam injection. The pressure of the helium neutral is about ten times less than that of the deuterium neutral.

The time evolution of helium density at $r/a=0.66$ with and without the divertor pump is compared in Fig. 4. The helium density, n_{He} , saturated about $8.0 \times 10^{17} \text{ m}^{-3}$ with the pump, while n_{He} kept increasing without the pump. The effective particle confinement time of helium, τ_{He}^* , is estimated to be 0.72 s. The energy confinement time, τ_E , is 0.18 s. Thus, the ratio of τ_{He}^* to τ_E , becomes about 4, which satisfies the ITER requirement of $\tau_{\text{He}}^*/\tau_E \leq 10$.¹⁴ The enrichment factor, $[P_{\text{He}}/(2P_{\text{D}_2})]/[n_{\text{He}}/n_e]$, at the pumping port behind the outer baffle plate is about 1, where P_{He} and P_{D_2} are the pressure of helium and deuterium, respectively. Since the profiles of helium and electron density are almost the same in the main plasma, the ratio n_{He}/n_e is almost equivalent to the ratio of the total helium particle to the total electron in the plasma, i.e., N_{He}/N_e . The obtained enrichment factor is 5 times larger than that obtained with an open divertor in JT-60.¹⁶ It was proved that the active fuel exhaust is very effective for the helium exhaust in the steady-state operation.

D. Long sustainment of ELMy H-mode plasmas

In 1996, quasi-steady-state operation of the high- β_p H-mode plasma for 2.6 s was carried out in the relatively broad pressure profile by slightly off-axis heating.¹² However, the problem with the quasi-steady-state high- β_p H-mode operation is that the recycling rate and impurity content increase for the long NBI pulse, when the integrated NBI input energy reaches above ~ 70 MJ, and causes the degradation of energy confinement. The control of neutrals and impurity is one of the important subjects of this year's campaign to achieve the ITER-like steady-state operation.

The low triangularity, δ (~ 0.15) and the high δ (~ 0.30) configurations are compared this year. The low δ operation has better exhaust efficiency in JT-60U, because a small "gap-in" can be obtained with this configuration. Also it is possible to keep the same plasma configuration during the NBI heating phase in low δ operation.

Figure 5 shows the demonstration of the long sustainment of the ELMy H mode with the divertor pump. The

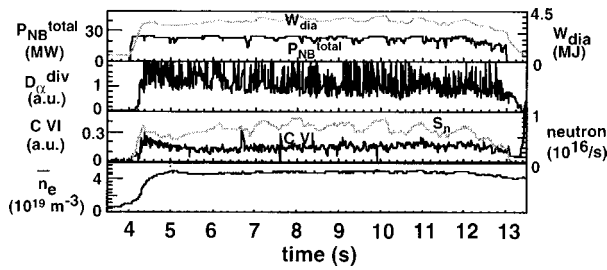


FIG. 5. Time evolution of NBI heating power, the diamagnetic stored energy, the intensity of divertor D_α , the intensity of carbon VI, the neutron emission rate, and the line-averaged density of the ELMy H mode. Long sustainment of the ELMy H mode for 9 s with the integrated NBI input energy of 203 MJ was performed without an increase in the recycling and carbon density.

plasma current and the toroidal field are 1.5 MA and 3.5 T, respectively. The line-averaged density is kept constant by the feedback control of the gas puff. The H factor ~ 1.7 and $\beta_N = 1.4-1.8$ is sustained for 9 s, which is much longer than the energy confinement time (several hundred milliseconds), and the effective particle confinement time (several seconds). Although the integrated NBI input energy reaches up to 203 MJ, no increase in D_α and C_{IV} line intensity can be seen with the divertor pump. Without divertor pumping the intensity of the D_α and C_{IV} line increases gradually with time like the results of the open divertor case.

E. Performance of ELMy H mode in the high-density regime

In JT-60U improved energy confinement has been demonstrated for the high ion temperature mode, that is $T_i(0) \gg T_e(0)$. In these plasmas, the gas puff fueling was not done during the NBI heating phase. The density normalized by the Greenwald limit, \bar{n}_e/n_{GW} , is 0.45 utmost. In order to study the density dependence of the H factor in ELMy H-mode plasmas, several series of ELMy H-mode plasmas with the different \bar{n}_e were examined. The high-density plasmas are obtained by the deuterium gas puff.

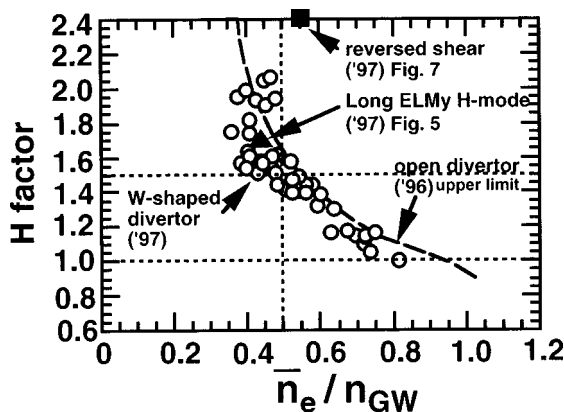


FIG. 6. Density dependence of the H factor based on ITER 89 power scaling in a W-shaped divertor (open circles) and an open divertor (broken line: upper limit) are compared in ELMy H mode plasmas. The plasma parameters are $I_p = 1.1-1.5$ MA, $B_t = 2.5-3.6$ T, $P_{NBI} = 22$ MW. The H factor decreases with the increase of density.

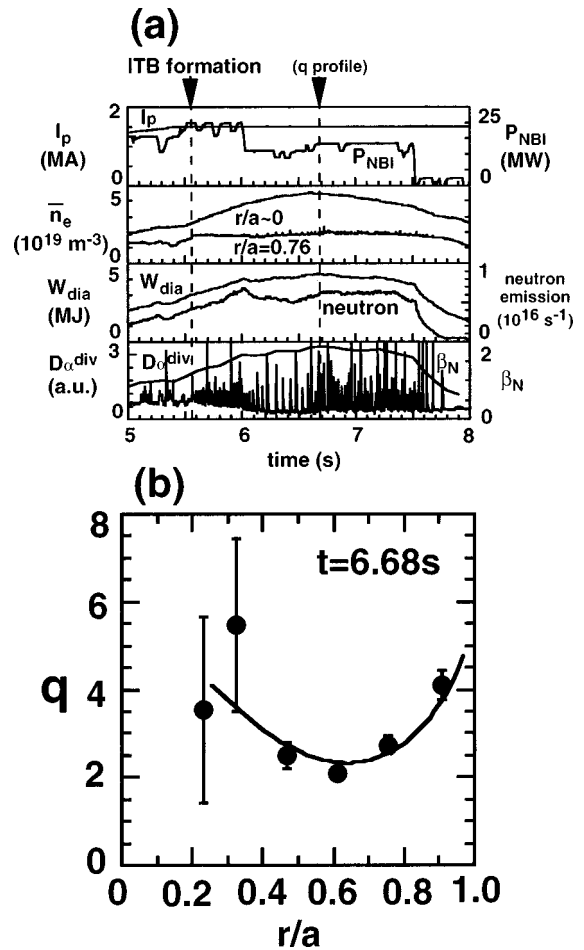


FIG. 7. (a) Time evolution of the plasma current, the NBI power, the line-averaged density, the diamagnetic stored energy, the neutron emission rate, and the intensity of divertor D_α for the ELMing reversed shear plasma. (b) The q profile at $t = 6.68$ s.

The density dependence of the H factor based on the ITER 89 power scaling is shown in Fig. 6. Open circles are the results of the W-shaped divertor. The region of plasma parameters are $I_p = 1.1-1.5$ MA, $B_t = 2.5-3.6$ T, and $P_{NBI} = 22$ MW. The H factor is about 1.5 at $\bar{n}_e/n_{GW} = 0.5$. These values, together with H factor=1, are indicated by dotted lines for convenience. The broken line denotes the upper limit of energy confinement by the open divertor. The data of the ELMy H-mode shot (shown in Fig. 5) and the reversed shear shot (shown in Fig. 7) are expressed by the closed triangle and square, respectively, for reference.

In spite of the divertor pump and the control of gap-in, the H factor degrades with the increase of density. Around $\bar{n}_e/n_{GW} = 0.6$, an X-point MARFE (multifaceted asymmetric radiation from the edge) occurs, which is a slightly smaller density range compared with the results of the open divertor. No improvement of energy confinement is found above $\bar{n}_e/n_{GW} = 0.8$. The density dependence of the H-factor is almost the same as the results of the open divertor, in which high-density operations were also carried out by gas puff fueling.¹⁷ The tendency mentioned above is not influenced by the position of gas puffing (from the main plasma, from behind the baffle plate), the ‘‘gap-in’’ and the distance be-

tween the baffle plate and the separatrix. The control of neutrals under the excess gas puff fueling from the main plasma for the high-density operation has not yet been optimized. The continuous pellet injection (centrifugal pellet injection) is planned to reduce neutrals.

III. STUDIES OF REVERSED SHEAR PLASMAS

A. ELMy H mode reversed shear plasmas

Reversed shear plasmas were obtained by the fast current ramp-up during the NBI heating phase. In these enhanced confinement plasmas ITB was seen in n_e , T_e , and T_i profiles just inside the minimum q surface. One of the merits of reversed shear operation is that a large energy confinement time is achieved. Moreover, the large portion of stored energy is the thermal stored energy, which is a reactor-like property. On the other hand, most of the good confinement shots in the reversed shear configuration ended with major disruption caused by the kink-ballooning mode.¹⁸ Moreover, there was no H-mode transition in high- B_t operation and the density and temperature in the plasma peripheral region outside the ITB remained low.

For the better performance of reversed shear plasmas, the improvement of energy confinement in the plasma peripheral region by the L–H transition is necessary. In order to avoid the high- β_p disruption caused by the huge pressure gradient within the thin ITB layer, careful and moderate NBI injection has been carried out in the operation. Just after the ITB formation, NBI heating power was stepped down, and the quasi-steady-state ELMy H mode plasmas were successfully obtained keeping the ITB.

Figure 7(a) shows the time evolution of the plasma parameters in the ELMing reversed shear shot with $I_p = 1.5$ MA, $B_t = 3.5$ T. At about $t = 5.55$ s, ITB begins to evolve. The central density starts to increase, while the edge density remains almost constant. At $t = 6.0$ s, eight units of NBI were reduced to five units. What is very interesting is that the stored energy, W_{dia} , did not decrease with the step-down of NBI power. The H factor ~ 2.4 and $\beta_N = 1.7$ – 1.9 was achieved with $\bar{n}_e/n_{\text{GW}} \sim 0.54$.

In this shot the L–H transition is not clear; i.e., there is no clear drop of D_α intensity. The relation of the timing between the ITB formation and the L–H transition is under investigation.

Figure 7(b) shows the q profiles measured by motional Stark effect (MSE). The position of minimum q is located about $r/a = 0.6$. The ITB is located just inside the q_{min} . Figure 8(a) shows the profiles of n_e , T_e , and T_i at $t = 6.5$ s. They had similar features in profile: a very steep gradient at the ITB and a relatively flat profile in the core region enclosed by the ITB. This feature remains until the end of NBI heating. In the peripheral region outside the ITB, the volume-averaged density, $\langle n_e \rangle$, the particle-averaged electron and ion temperature, $\langle T_e \rangle$ and $\langle T_i \rangle$, become large due to the H mode transition. These averaged values in the peripheral region are almost the same or above those of the non H-transition shot of $I_p = 2.8$ MA with $Q_{\text{DT}}^{\text{eq}} = 1.05$.

Figure 8(b) shows the power deposition profile of NBI heating, Ohmic heating and radiation loss profiles. The NBI

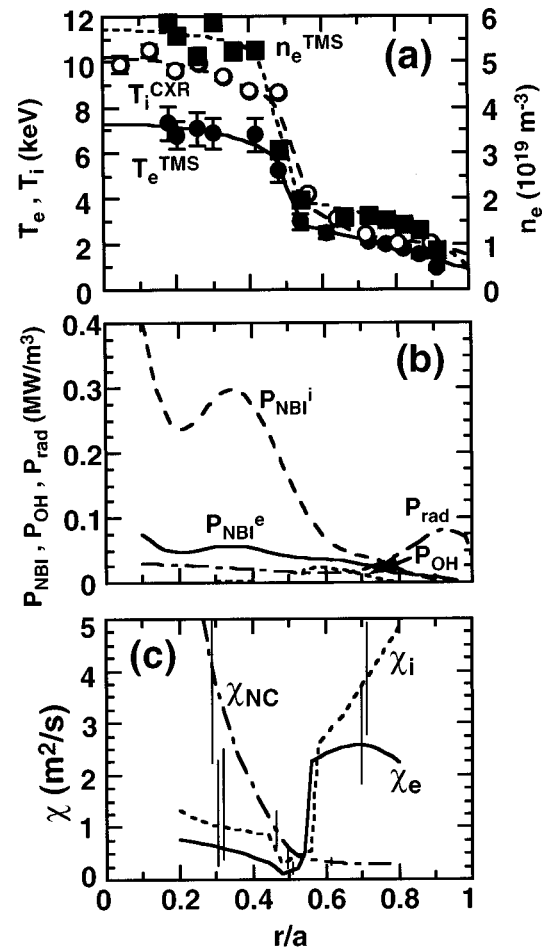


FIG. 8. Profiles of (a) n_e, T_e, T_i , (b) NBI heating power, P_{NBI}^e and P_{NBI}^i , Ohmic heating power, P_{OH} , radiation loss, P_{rad} , and (c) thermal diffusivity, χ_e and χ_i , and the neoclassical diffusivity, χ_{NC} , in the ELMing reversed shear plasma.

heating profiles are calculated by an orbit following the Monte Carlo (OFMC) code.¹⁹ The ripple loss of fast ion is about 7% of the injected NBI. Figure 8(c) shows the profiles of electron and ion thermal diffusivity, χ_e and χ_i , and the neoclassical diffusion, χ_{NC} . Both χ_e and χ_i are very small inside the thin ITB layer. In the core region enclosed by ITB, both χ_e and χ_i are the same level or smaller than the χ_{NC} . This transport feature is the same as that obtained in the transient phase.

B. Study of microinstabilities around the ITB

A large pressure gradient within the thin ITB layer is a distinctive feature for the reversed shear plasmas in JT-60U, which has a potential to be a free energy source to excite microinstabilities. The linear growth rate of high- n toroidal drift modes was analyzed by a linear toroidal kinetic microinstability analysis code, the FULL code in collaboration with the Princeton Plasma Physics Laboratory (PPPL).^{20,21} By changing the $k_\theta \rho_i$ value, where k_θ is a wave number in the poloidal direction and $\rho_i = \sqrt{m_i T_i / e B}$ is an ion Larmor radius, the largest linear growth rate, γ_L , is calculated locally, not including the rotational effects. As for the suppression

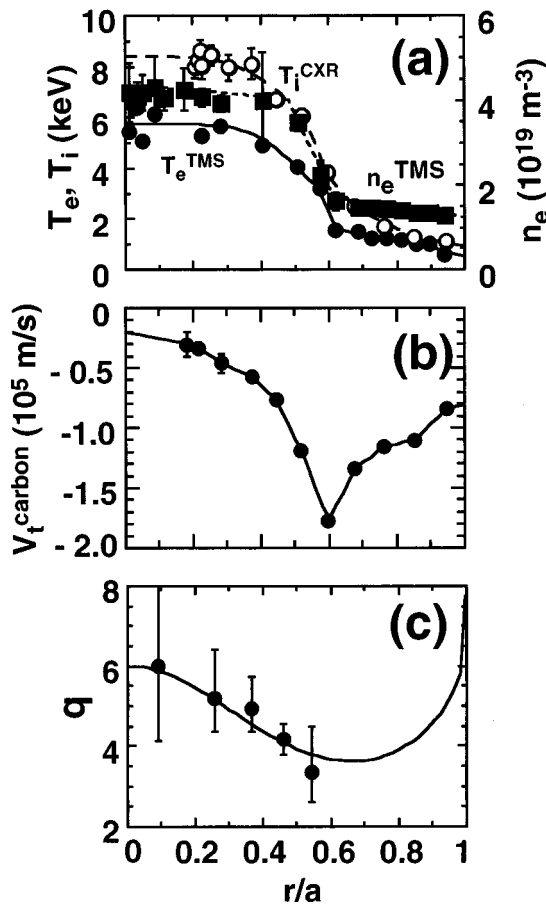


FIG. 9. Profiles of (a) n_e, T_e, T_i , (b) toroidal rotation, V_t , and (c) q measured by MSE for the reversed shear shot E24715 ($I_p=1.2$ MA and $B_t=3.5$ T).

mechanism for the microturbulence, the $E \times B$ flow shear is regarded as playing an important role.²² The radial electric field and the $E \times B$ shearing rate, $\omega_{E \times B}$, are estimated by solving the neoclassical parallel momentum balance equations with the measured toroidal rotation profile of the carbon impurity.

The reversed shear plasma with $I_p=1.2$ MA and $B_t=3.5$ T was examined. Profiles of n_e, T_e, T_i, q , and the toroidal rotation speed of carbon, V_t , are shown in Fig. 9. Then profiles of γ_L and $\omega_{E \times B}$ are calculated for these profiles (Fig. 10). It was found that the microinstability is localized around the thin ITB layer. Within the ITB layer, the dominant mode is the toroidal drift mode (the trapped electron η_i mode).²³ This mode is roughly stabilized by the $E \times B$ shearing rate, i.e., $\gamma_L \leq \omega_{E \times B}$.

The local stability analysis predicted that this microinstability would be stable in the plasma peripheral region because of the fairly flat pressure profile. Actually, the thermal diffusivity in this region is far larger than the neoclassical diffusion. The origin of anomalous transport in this region is the next subject to be clarified.

C. Study of reduced transport inside minimum- q region

As shown in Fig. 8(c), the reduced transport within the thin ITB layer is a distinctive feature of reversed shear plas-

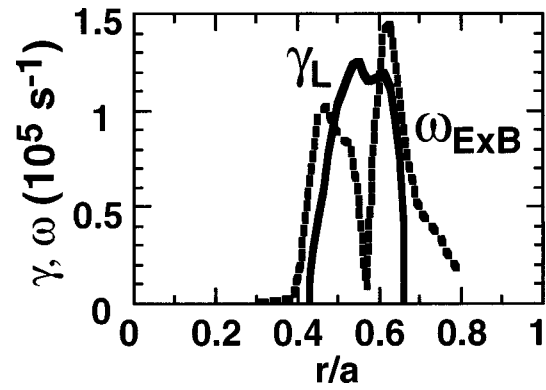


FIG. 10. Profiles of the linear growth rate of, γ_L (solid line) and the $E \times B$ shearing rate, $\omega_{E \times B}$ (dotted line).

mas in JT-60U. A full toroidal geometry particle simulation code (TPC) is used to clarify the mode structure around ITB.^{24,25} The instability with poloidal mode number m and toroidal mode number n , which occurred at the rational surface $q=m/n$, can be coupled to other modes $(m+j, n)$ (j is an integer) by the toroidal mode coupling and create a non-local or semiglobal structure of turbulence, which extends in the minor radial direction. In the case of the reversed shear configuration, the distance between the rational surfaces of adjacent modes becomes large at the minimum q surface. Thus, when the q_{\min} surface is located between the adjacent mode rational surfaces, these modes become isolated from each other.

Figure 11 shows the contour of electrostatic potential in the poloidal cross section. At the q_{\min} surface indicated by the solid line, the semiglobal mode structure is broken up. Actually, the energy of mode, $\sum_m [\phi_m]^2$, has discontinuity at q_{\min} . This discontinuous structure is regarded as a candidate of the reduced radial transport across the ITB layer.

IV. OTHER STUDIES FOR ITER PHYSICS R&D

A. Studies of halo current

The electromagnetic force driven by the halo current is an important decision factor in ITER design. Therefore, the study of halo current characteristics is regarded as one of the most important subjects in ITER physics R&D. Up to the present time, the experimental data on the halo current mainly came from the middle- and small-sized tokamaks and the database from large tokamaks is insufficient. During the divertor modification, Rogovsky coils were newly installed to measure the halo current precisely.

The VDE (Vertical Displacement Event) was simulated by pushing the plasma column downward toward the X point. The halo current flows into the inside baffle plates, runs in the vacuum vessel and goes back out from the outside baffle plates, when the direction of both the plasma current and the toroidal field is clockwise. The halo current becomes highest when dI_p/dt takes the maximum value during the current quench. Experimental results show that the maximum value of $I_{\text{halo}}/I_p \times \text{TPF}$ is smaller than that of middle-sized devices, where the toroidal peaking factor (TPF) means

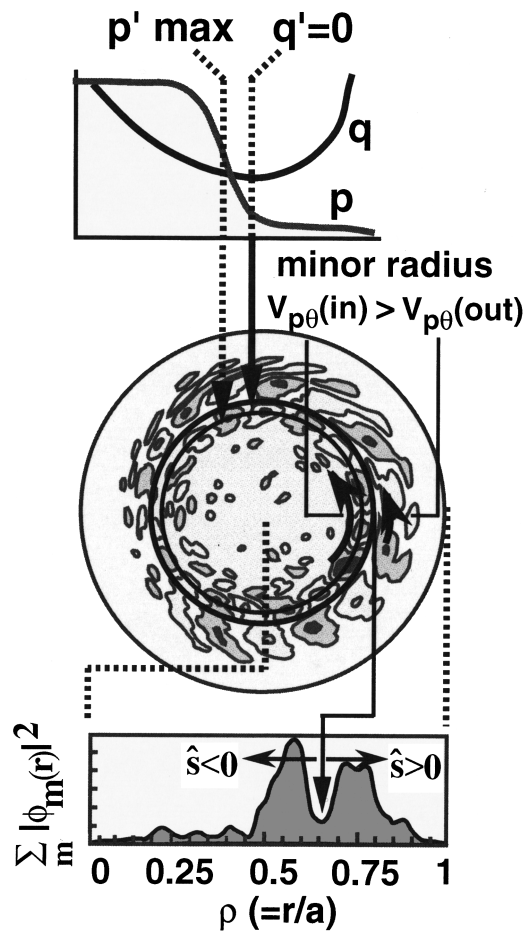


FIG. 11. Contours of electrostatic potential in the reversed shear configuration. Discontinuity occurs in the mode structure at the q_{\min} surface.

the scale of spatial variation of the halo current in the toroidal direction. The physical mechanism of the halo current will be investigated in the future.

B. Studies of TAE mode

Toroidicity-induced Alfvén Eigenmode (the TAE mode) is regarded as unfavorable for the confinement of α particles. It is therefore necessary to study the characteristics of the TAE mode and the method to stabilize it. The TAE mode was observed by the second harmonic ICRF (the ion cyclotron range of frequencies) minority heating in JT-60U²⁶ This year N-NBI was applied to excite the TAE mode.

The N-NBI alone with 350 keV beam energy and 3 MW beam power was injected into the plasma with $I_p = 0.7$ MA, $B_t = 1.54$ T for 0.4 s. The parallel velocity of beam, V_{\parallel} , at the tangency radius is 4.4×10^6 m/s. The Alfvén velocity, V_A , which is estimated by the line-averaged density of the CO₂ interferometer in the central chord and the magnetic field at the magnetic axis is $(7.1-8.2) \times 10^6$ m/s. The range of V_A value comes from the slight decrease of the density during N-NBI. Thus, V_{\parallel}/V_A is 0.54–0.62. Just after the beginning of N-NBI injection, a TAE-like high-frequency magnetic fluctuation of ~ 50 kHz (toroidal mode number $n = 1$) and ~ 100 kHz ($n = 2$) occurs. At the burst of magnetic fluctuation, a small drop of the neutron emission rate by

2%–3% was observed. The volume-averaged fast ion beta is estimated at about 0.2%, which is less than the fast ion beta value of 0.5% for the TAE mode excitation obtained experimentally in TFTR (Tokamak Fusion Test Reactor)²⁷ and DIII-D.²⁸ The different threshold beta value is studied from the viewpoint of the fast ion density profile. Also, the possibility of another beam-driven mode, the “chirping mode” observed in DIII-D, is considered.²⁹

V. SUMMARY

JT-60U experiments with the W-shaped divertor configuration have been successfully carried out. The effective removal of helium introduced by a beam was demonstrated. The value of τ_{He}^*/τ_E became about 4. The enrichment factor of helium increased by a factor of 5 compared with the results of the open divertor. The long sustainment of ELMy H mode phase was demonstrated by the divertor pump for 9 s. No increase of recycling or impurity density were observed with the integrated NBI input energy of 203 MJ. The performance of high-density ELMy H mode plasmas operated by strong gas puff fueling degraded near the Greenwald limit.

Steady-state ELMy H-mode plasmas in the reversed shear configuration were obtained for the first time. The stability of high- n toroidal drift modes was analyzed by the FULL code, the linear toroidal kinetic microinstability analysis code, in collaboration PPPL. The $E \times B$ shearing rate, derived from experimental measurements, is sufficient to suppress the trapped-electron- η_i mode, which has been predicted to be the dominant microinstability in the vicinity of the ITB. The toroidal particle simulation code predicts the reduction of radial transport across the ITB, which is located inside the q_{\min} position.

The precise measurement of the halo current at VDE was carried out. A TAE-like mode has been observed by N-NBI injection for the first time.

In the campaign for next year, we plan to demonstrate the full noninductive current drive with high I_p (over 2 MA) and a high \bar{n}_e condition with the increase of N-NBI injection power. The optimization of the partial detached radiative divertor will be carried out for both the normal shear and the reversed shear operations. The optimization of the reversed shear plasmas and high- β_p H mode plasmas will be performed for the study of improved performance.

ACKNOWLEDGMENTS

We would like to express our appreciation to researchers who visit JT-60U under a wide range of international collaboration programs, for their valuable suggestion, comments and contributions. We are very grateful to Dr. K. McGuire, Dr. J. Manickam, and Dr. S. Sabbagh of the Princeton Plasma Physics Laboratory (PPPL) for fruitful discussion through the remote experimental participation. The discussion of the $E \times B$ shearing rate with Dr. T. S. Hahm of PPPL is greatly acknowledged.

APPENDIX: THE JT-60 TEAM

H. Adachi, H. Akasaka, K. Akiba,* N. Akino, K. Annou, T. Arai, K. Arakawa, N. Asakura, M. Azumi, M. Bell,* B. M. Bernholz,* R. Budny,* J. Cao,* C. Z. Cheng,* S. Chiba, O. Da Costa,* N. Ebisawa, Y. Fang,* G. Y. Fu,* T. Fujii, T. Fujita, H. Fukuda,* H. Fukuda,* T. Fukuda, A. Funahashi, H. Furukawa,* X. Gao, L. Grisham,* S. Gunji, K. Haga,* H. Haginoya,* K. Hamamatsu, T. Harano,* Y. Hasegawa,* T. Hatae, N. Hayashi,* S. Higashijima, K. Hill,* H. Hiratsuka, S. Hiranai, T. Hirayama, T. Hiroi,* A. Hirose,* A. Honda, M. Honda, B. G. Hong,* R. M. Hong,* N. Hosogane, S. Hudson,* H. Ichige, S. Ide, Y. Ikeda, M. A. Inoue, Isaka, A. Isayama, N. Isei, S. Ishida, K. Ishii,* Y. Ishii, T. Ishijima,* K. Itami, T. Itoh, Y. Iwase, T. Iwahashi, Y. Kamada, A. Kaminaga, T. Kashiwabara, M. Kawai, Y. Kawamata, Y. Kawano, M. Kawanobe,* D. Kazama, M. Kazawa, E. Kaziyama,* M. Kikuchi, H. Kimura, T. Kimura, H. Kishimoto, Y. Kishimoto, S. Kitamura, K. Kiyono, K. Kodama, Y. Koide, M. Koiwa,* S. Kokusen, K. Komuro,* T. Kondoh, S. Konoshima, J. Koog,* G. J. Kramer,* H. Kubo, A. Kumagai,* K. Kurihara, G. Kurita, M. Kuriyama, M. Kusaka,* Y. Kusama, L. Lao,* C. Liu,* A. Makhankov,* K. Masaki, T. Matsuda, T. Matsumoto, M. Matukawa, B. E. Mills,* T. Miura, Y. M. Miura, N. Miya, K. Miyachi, H. Miyata,* Y. Miyo, K. Mogaki, M. Mori, M. Morimoto,* A. Morioka, S. Moriyama, M. Nagami, A. Nagashima, K. Nagashima, S. Nagaya, O. Naito, Y. Nakamura, R. Nazikian,* H. Nemoto, M. Nemoto, S. V. Neudatchin,* Y. Neyatani, T. Nishitani, H. Nobuska,* N. Ogiwara, T. Ohga, M. Ohsawa,* K. Ohshima,* T. Ohshima, T. Oikawa, T. Okabe, J. Okano, K. Omori, S. Omori, Y. Omori, Y. Onose, T. Ooba,* H. Oohara, T. Ozeki, A. Polevoi,* R. Ramakrishnan,* G. Rewoldt,* M. Saidoh, M. Saigusa,* N. Saito, A. Sakasai, S. Sakata, T. Sakuma, S. Sakurai, T. Sasajima, N. Sasaki,* T. Sato,* G. Schilling,* S. D. Scott,* M. Seimiya, H. Seki, M. Seki, M. Shibayama,* M. Shimada, K. Shimizu, M. Shimizu, M. Shimon, K. Shinohara, S. Shinozaki,* M. Shitomi, K. Sukanuma, T. Sugie, H. Sunaoshi, M. Suzuki,* S. Suzuki,* M. Takahashi, S. Takahashi, S. Takahashi,* S. Takeji, H. Takenaga, T. Takenouchi,* T. Takizuka, H. Tamai, Y. Tanai,* T. S. Taylor,* F. V. Tchernychev,* M. Terakado, T. Terakado, K. Tobita, S. Tokuda, T. Totsuka, R. Toyokawa, N. Toyoshima, K. Tsuchiya, T. Tsugita, Y. Tsukahara, T. Tsuruoka,* T. Tuda, K. Uehara, Y. Uramoto, H. Usami,* K. Ushigusa, K. Usui, J. Van Dam,* G. Wurden,* J. Yagyu, M. Yamagiwa, T. Yamamoto, O. Yamashita, K. H. Yamazaki,* L. Yan,* K. Yokokura, H. Yoshida, M. Yoshida, R. Yoshino. Asterisk (*) indicates staff other than JAERI.

¹Y. Koide and the JT-60 Team, *Phys. Plasmas* **4**, 1623 (1997).

²M. Kikuchi, H. Shirai, T. Takizuka, Y. Kamada, Y. Koide, H. Yoshida, O. Naito, T. Fujita, T. Nishitani, N. Isei, M. Sato, T. Fukuda, S. Tsuji, H. Kubo, T. Sugie, N. Asakura, N. Hosogane, H. Nakamura, M. Shimada, R. Yoshino, H. Ninomiya, M. Kurihara, M. Yagi, K. Tani, A. A. A. van Blokland, T. S. Taylor, G. L. Jackson, D. J. Campbell, D. Stork, A. Tanga, and JT-60 Team, in *Proceedings of the 14th International Conference on Plasma Physics and Controlled Nuclear Fusion Research*, Würzburg, 1992 (International Atomic Energy Agency, Vienna, 1993), Vol. 1, p. 189.

³Y. Koide, S. Ishida, M. Kikuchi, M. Mori, S. Tsuji, T. Nishitani, Y. Kawano, T. Hatae, T. Fujita, T. Fukuda, T. Ozeki, H. Shirai, Y. Kamada,

R. Yoshino, H. Ninomiya, M. Azumi, and the JT-60 Team, in *Proceedings of the 15th International Conference on Plasma Physics and Controlled Nuclear Fusion Research*, Seville, 1994 (International Atomic Energy Agency, Vienna, 1995), Vol. 1, p. 199.

⁴T. Fujita, S. Ide, H. Shirai, M. Kikuchi, O. Naito, Y. Koide, S. Takeji, H. Kubo, and S. Ishida, *Phys. Rev. Lett.* **78**, 2377 (1997).

⁵R. Aymar, V. Chuyanov, M. Huguet, R. Parker, Y. Shimomura, and the ITER Joint Central Team and Home Teams, in *Proceedings of the 16th International Conference on Fusion Energy*, Montréal, 1996 (International Atomic Energy Agency, Vienna, 1997), Vol. 1, p. 3.

⁶S. Ishida, Y. Neyatani, Y. Kamada, A. Isayama, T. Fujita, Y. Oikawa, Y. Koide, Y. Kawano, H. Shirai, T. Ozeki, T. Nishitani, S. Takeji, H. Kimura, T. Hatae, T. Fukuda, N. Isei, and the JT-60 Team, in Ref. 5, Vol. 1, p. 315.

⁷S. Ishida, T. Fujita, H. Akasaka, N. Akino, K. Annou, T. Aoyagi, T. Arai, K. Arakawa, N. Asakura, M. Azumi, R. Budny, S. Chiba, O. Da Costa, N. Ebisawa, T. Fujii, T. Fukuda, A. Funahashi, L. Grisham, S. Gunji, K. Hamamatsu, Y. Hasegawa, T. Hatae, S. Higashijima, H. Hiratsuka, S. Hirauchi, T. Hirayama, A. Honda, M. Honda, N. Hosogane, H. Ichige, S. Ide, Y. Ikeda, M. Isaka, A. Isayama, N. Isei, Y. Ishii, N. Isozaki, K. Itami, T. Itoh, T. Iwahashi, Y. Kamada, A. Kaminaga, T. Kashiwabara, M. Kawai, Y. Kawamata, Y. Kawano, D. Kazama, M. Kazawa, M. Kikuchi, H. Kimura, T. Kimura, H. Kishimoto, Y. Kishimoto, S. Kitamura, K. Kiyono, K. Kodama, Y. Koide, S. Kokusen, T. Kondoh, S. Konoshima, J. Koog, G. J. Kramer, H. Kubo, K. Kurihara, G. Kurita, M. Kuriyama, Y. Kusama, K. Masaki, T. Matsuda, T. Matsumoto, M. Matukawa, T. Miura, N. Miya, K. Miyachi, H. Miyata, Y. Miyo, K. Mogaki, M. Mori, M. Morimoto, A. Morioka, S. Moriyama, M. Nagami, A. Nagashima, K. Nagashima, S. Nagaya, O. Naito, Y. Nakamura, M. Nemoto, Y. Neyatani, T. Nishitani, N. Ogiwara, T. Ohga, M. Ohsawa, T. Ohshima, T. Oikawa, T. Okabe, J. Okano, K. Omori, S. Omori, Y. Omori, Y. Onose, H. Oohara, T. Ozeki, M. Saidoh, M. Saigusa, N. Saito, A. Sakasai, S. Sakata, S. Sakurai, T. Sasajima, M. Sato, S. D. Scott, M. Seimiya, H. Seki, M. Seki, M. Shimada, K. Shimizu, M. Shimizu, M. Shimon, S. Shinozaki, H. Shirai, M. Shitomi, K. Sukanuma, T. Sugie, H. Sunaoshi, M. Takahashi, S. Takahashi, S. Takeji, H. Takenaga, T. Takizuka, H. Tamai, M. Terakado, T. Terakado, K. Tobita, S. Tokuda, T. Totsuka, Y. Toyokawa, N. Toyoshima, K. Tsuchiya, T. Tsugita, Y. Tsukahara, T. Tuda, Y. Uramoto, K. Ushigusa, K. Usui, J. Yagyu, M. Yamagiwa, M. Yamamoto, T. Yamamoto, O. Yamashita, K. Yokokura, H. Yoshida, M. Yoshida, and R. Yoshino, *Phys. Rev. Lett.* **79**, 3917 (1997).

⁸S. Sakurai, N. Asakura, K. Itami, Y. Kamada, H. Kubo, and A. Sakasai, in *Proceedings of the 1996 International Conference on Plasma Physics*, Nagoya, 1996 (The Japan Society of Plasma Science and Nuclear Fusion Research, Nagoya, 1997), Vol. 1, p. 646.

⁹M. Kuriyama, N. Akino, T. Aoyagi, N. Ebisawa, Y. Fujiwara, N. Isozaki, A. Honda, T. Inoue, T. Itoh, M. Kawai, M. Kazawa, J. Koizumi, K. Miyamoto, N. Miyamoto, K. Mogaki, Y. Ohara, T. Ohga, Y. Okumura, H. Oohara, K. Oshima, F. Satoh, H. Seki, T. Takenouchi, Y. Toyokawa, K. Usui, K. Watanabe, M. Yamamoto, and T. Yamazaki, in *Proceedings of the 19th Symposium on Fusion Technology*, Lisbon, 1996 (North-Holland, Amsterdam, 1997), p. 693.

¹⁰S. Ide, O. Naito, T. Fujita, T. Oikawa, M. Seki, and the JT-60 team, in Ref. 5, Vol. 3, p. 253.

¹¹M. Kikuchi and M. Azumi, *Plasma Phys. Controlled Fusion* **37**, 1215 (1995).

¹²Y. Kamada, R. Yoshino, K. Ushigusa, Y. Neyatani, T. Oikawa, O. Naito, S. Tokuda, H. Shirai, T. Takizuka, T. Ozeki, M. Azumi, T. Hatae, T. Fujita, S. Takeji, M. Matukawa, Y. Koide, T. Fukuda, S. Ishida, and JT-60 Team, in Ref. 5, Vol. 1, p. 247.

¹³N. Hosogane, S. Sakurai, K. Shimizu, S. Tsuji-Iio, M. Shimada, K. Kodama, K. Masaki, N. Asakura, K. Itrami, and T. Takizuka, in Ref. 5, Vol. 3, p. 555.

¹⁴G. Janeschitz, H. D. Pacher, G. Federici, Y. Iglikhanov, A. Kukushkin, E. Martin, O. Post, M. Sugihara, R. Tivey, T. Ando, A. Antipenkov, S. Chiochio, S. Hiroki, P. Ladd, H. Nakamura, P. Parker, and K. Schaubel, in Ref. 5, Vol. 2, p. 755.

¹⁵A. Sakasai, H. Kubo, N. Hosogane, T. Sugie, S. Higashijima, K. Itami, N. Asakura, Y. Koide, K. Shimizu, S. Sakurai, M. Shimada, S. Tsuji, and the JT-60 Team, in Ref. 3, Vol. 2, p. 95.

¹⁶H. Nakamura, T. Hirayama, Y. Koide, K. Tobita, K. Tani, T. Fukuda, H. Kubo, M. Kuriyama, Y. Kusama, A. Sakasai, T. Sugie, and H. Yoshida, *Phys. Rev. Lett.* **67**, 2658 (1991).

- ¹⁷N. Asakura, K. Shimizu, H. Shirai, Y. Koide, and T. Takizuka, *Plasma Phys. Controlled Fusion* **39**, 1295 (1997).
- ¹⁸T. Ozeki, M. Azumi, Y. Ishii, Y. Kishimoto, G. Y. Fu, T. Fujita, G. Rewoldt, M. Kikuchi, Y. Kamada, H. Kimura, Y. Kusama, M. Saigusa, S. Ide, and H. Shirai, *Plasma Phys. Controlled Fusion* **39**, A371 (1997).
- ¹⁹K. Tani, M. Azumi, and H. Kishimoto, *J. Phys. Soc. Jpn.* **50**, 1726 (1981).
- ²⁰G. Rewoldt, W. M. Tang, and M. S. Chance, *Phys. Fluids* **25**, 480 (1982).
- ²¹G. Rewoldt, W. M. Tang, S. Kaye, and J. Menard, *Phys. Plasmas* **3**, 1667 (1996).
- ²²T. S. Hahm and K. H. Burrell, *Plasma Phys. Controlled Fusion* **38**, 1427 (1996).
- ²³G. Rewoldt and W. M. Tang, *Phys. Fluids B* **2**, 318 (1990).
- ²⁴Y. Kishimoto, J.-Y. Kim, T. Fukuda, S. Ishida, T. Fujita, T. Tajima, W. Horton, G. Furnish, and M. J. LeBrun, in Ref. 5, Vol. 2, p. 581.
- ²⁵Y. Kishimoto, T. Tajima, W. Horton, M. J. LeBrun, and J. Y. Kim, *Phys. Plasmas* **3**, 1289 (1996).
- ²⁶H. Kimura, S. Moriyama, M. Saigusa, Y. Kusama, T. Ozeki, G. J. Kramer, T. Fujita, T. Oikawa, T. Fujii, M. Nemoto, K. Hamamatsu, O. DaCosta, S. Ishida, Y. Kamada, T. Kondoh, A. Morioka, Y. Neyatani, K. Tobita, V. I. Afnessiev, and the JT-60 team, in Ref. 5, Vol. 3, p. 295.
- ²⁷K. L. Wong, R. J. Fonck, S. F. Paul, D. R. Roberts, E. D. Fredrickson, R. Nazikian, H. K. Park, M. Bell, N. L. Bretz, R. Budny, S. Cohen, G. W. Hammett, F. C. Jobes, D. M. Meade, S. S. Medley, D. Mueller, Y. Nagayama, D. K. Owens, and E. J. Synakowski, *Phys. Rev. Lett.* **66**, 1874 (1991).
- ²⁸E. J. Strait, W. W. Heidbrink, A. D. Turnbull, M. S. Chu, and H. H. Duong, *Nucl. Fusion* **33**, 1849 (1993).
- ²⁹W. W. Heidbrink, *Plasma Phys. Controlled Fusion* **37**, 937 (1995).